Available online at www.sciencedirect.com
ScienceDirect
Polymer 48 (2007) 7211–7220
polymer
www.elsevier.com/locate/polymer

Simulation of mechanical properties of oriented glassy polystyrene

Frederick E. Bernardin III, Gregory C. Rutledge*

Department of Chemical Engineering, Massachusetts Institute of Technology, Cambridge, MA 02139-4301, United States

Received 20 August 2007; received in revised form 21 September 2007; accepted 24 September 2007
Available online 29 September 2007

Abstract

Mechanical properties of processed polymers depend sensitively on their microstructure. In order to understand how different processing conditions affect the mechanical properties of polymers, one needs a means to describe the process-induced microstructure. Because the characteristic relaxation times of processed polymer chains often span several orders of magnitude, it is commonly the case that partial relaxation of the chains is frozen into the final product. We report results of molecular simulations by the Semi-Grand Canonical Monte Carlo (SGMC) method to study the orientation-dependent elasticity of glassy polystyrene as a function of both the system-average degree of orientation and the degree of relaxation of chain ends at a constant average orientation, in accord with the tube model of Doi and Edwards. Our simulations reproduce quantitatively the experimentally observed trends in the tensile modulus E_{11} as a function both of the system-average orientation and of the inhomogeneity of the orientation along the chain due to rapid relaxation of chain ends. The results show that the partial relaxation of the polymer chains is sufficient to explain the observed variation of mechanical properties for samples that differ in processing history, yet have the same observed birefringence.

Keywords: Polystyrene; Elastic modulus; Molecular simulation

1. Introduction

A useful characteristic of polymeric materials is their processability into persistent, non-equilibrium structures that exhibit anisotropic mechanical and optical properties. For example, Hadley and coworkers showed that by subjecting polymer filaments to a draw ratio of approximately 6, one obtains an order-of-magnitude increase in the tensile modulus of low-density and high-density polyethylenes, polypropylene, and polyethylene terephthalate [1]. Other polymers follow the same trend, albeit with less dramatic increases in their tensile properties [1,2].

We have previously studied polymer systems that are homogeneously oriented, both spatially and along the chain contour [3,4] using the Semi-Grand Canonical Monte Carlo (SGMC) method [5]. Using this approach, many aspects of dense polymer systems that are out of equilibrium can be inferred from simple structural measurements like birefringence. These include stress–optical relationships, average macromolecular conformations, and enthalpic and entropic contributions to the changes in free energy upon orientation. These homogeneously oriented simulations are appropriate for the local description of systems exhibiting macroscopic gradients in orientation, provided that the average orientation and stresses are effectively constant at the local (nanometer) scale. In such cases, the simulated homogeneous systems should be viewed as representative volume elements (RVEs) of the larger, spatially heterogeneous system. Such an approach can be readily used to investigate the spatial variation in, e.g., the orientation of injection-molded parts [6].

However, in some cases a difference in chain relaxation times leads to molecules or parts of molecules that are oriented to different degrees even within a typical RVE, which therefore cannot be adequately described using a series of simulations with homogeneous orientation. One example of this inhomogeneity is the enhanced orientation of long chains *vis-à-vis* short

* Corresponding author.
E-mail address: rutledge@mit.edu (G.C. Rutledge).

0032-3861/$ - see front matter © 2007 Elsevier Ltd. All rights reserved.
doi:10.1016/j.polymer.2007.09.034

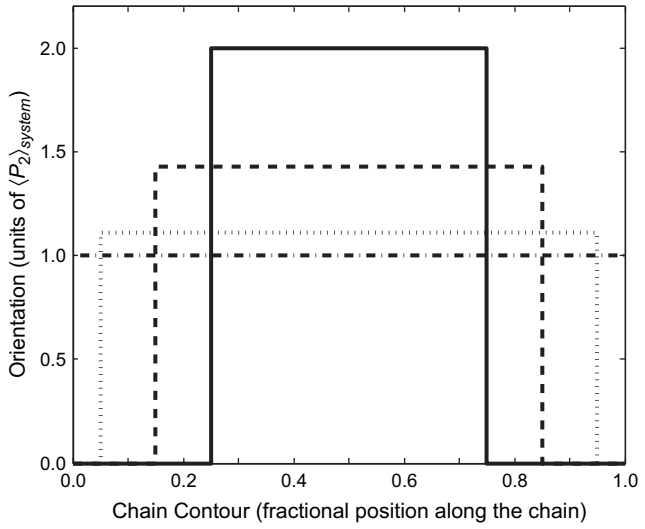

Fig. 1. Schematic diagram of the inhomogeneous distribution of orientation along the chain contour, as proposed in Ref [8]. f is the fraction of the chain whose orientation has been completely lost due to chain relaxation; see text for details. $f = 0.0$ (dot-dashed line), 0.1 (dotted line), 0.3 (dashed line), and 0.5 (solid line) for partial relaxation of the chain. While the curves represent different distributions of orientation, the overall average orientation $<P_2>_{system}$ is the same for all of the curves.

chains during flow-induced crystallization of polyethylene [7], which is believed to be responsible for the ''shish–kebab'' morphology.

The simulations presented here explore another example of inhomogeneity – the variation of orientation along the contour of individual polymer chains. The current simulations were prompted by the results of a study of the effects of draw ratio and temperature on the development of orientation in atactic polystyrene (PS), and the resulting effects on the mechanical properties, by De Francesco and Duckett [8,9]. Based on the theories of contour-dependent relaxation of oriented polymer chains published by Doi [10] and by Milner et al. [11], De Francesco and Duckett concluded that the variation in the mechanical properties could be explained by the inhomogeneity of the orientation along the chain contour, as illustrated in Fig. 1 (similar to Fig. 6 of Ref. [8]). The inhomogeneity arises from the fact that the chain relaxation propagates from the chain ends toward the center of the chain. Because the longest and shortest time scales of relaxation for polymer systems span many orders of magnitude, partial relaxation is a common feature of polymeric systems.

Although the study of polymer systems out of equilibrium normally entails simulation of the real dynamics of the polymer, the longest time scales for most polymers are not amenable to molecular dynamics (MD) simulation without substantial coarse-graining. While this coarse-graining may allow the exploration of polymer dynamics on the desired time scale, this comes with the loss of the unique chemical characteristics of the system, which are important for the accurate calculation of mechanical and rheological properties. In such cases, the use of a constrained Monte Carlo (MC) simulation offers an alternative approach to study a system far from equilibrium.

In the same way that we have used the SGMC method to provide a thermodynamically consistent ensemble to describe homogeneous states of orientation, we can also model systems that describe inhomogeneous states of orientation. This is achieved by applying an orientation potential selectively to a subset of segments within the chains, chosen according to criteria such as the length of chain in which such segments reside, or the contour distance of the segment from a chain end. This allows us to create simulations that can readily explore the evolution of microstructure and the dependence of properties like Young's modulus on such evolution. The resulting ensembles can also serve as a starting point for subsequent MD simulations of dynamic phenomena such as crystallization. Here, we focus on the dependence of mechanical properties of glassy polystyrene on process-induced orientation of either a homogeneous or inhomogeneous nature.

2. Theoretical approach

2.1. Physics of chain relaxation

The Doi–Edwards theory [12] has been successful in explaining a number of observed dynamic phenomena of polymer chains. It is built upon a ''tube'' model that envisions an individual polymer chain as being constrained by entanglements with other chains to remain within a tube that follows the contour of the chain. The tube model establishes a number of characteristic times that explain various aspects of polymer dynamics. These include the entanglement time τ_e, the retraction time τ_r and the reptation time τ_d, where $\tau_e < \tau_r < \tau_d$. The entanglement time represents the characteristic time for equilibration of the density of polymer segments between entanglements; the retraction time characterizes the recoil after deformation of the tube contour to its original size, as well as fluctuation of the tube contour length at equilibrium; the reptation time characterizes the loss of memory of the original conformation of the tube.

Orientation of the polymer chains occurs when the Weissenberg number for reptation, the product of the strain rate and the reptation time $\dot{\gamma}\tau_d$, is greater than unity, thus giving rise to deformation of the tube. However, if the Weissenberg number for retraction, i.e., the product of the strain rate and the retraction time $\dot{\gamma}\tau_r$, is less than unity, two dynamic processes contribute to the loss of deformation-induced orientation through partial relaxation of the tube: (1) the aforementioned retraction of the chain decreases its tube contour length and attenuates the orientation of the entire molecule, and (2) fluctuations of the contour length (or ''breathing'' modes) eliminate orientation preferentially at the chain ends by allowing the ends of the molecule to escape from the tube on a time scale that is short compared to the reptation time τ_d. The result is that even in the absence of reptation ($\dot{\gamma} > 1/\tau_d$) there is a finite fraction of the chain that nevertheless escapes the tube and disorients on the shorter time scale of order τ_r. This effect was used by Doi to explain the value of 3.4 in the power law dependence of viscosity on molecular weight [10] and has also been used to correct other deviations of the Doi–Edwards (DE)

model from experimental data [13]. The scaling of this effect goes as the inverse square root of the number of entanglement lengths; a prefactor of 1.3 was estimated by Doi using a variational calculation of the Rouse model and accounting for deformation of the tube under strain [14]. This prefactor is consistent with other studies as well [15,16]. Thus, the fraction of the chain f that has lost orientation on the sub-τ_d time scale is:

$$f = 1.3\left(\frac{M_e}{M}\right)^{0.5} \quad (1)$$

where M_e and M are the entanglement molecular weight and chain molecular weight, respectively.

The simplest way in which to model the partial loss of orientation at the molecular scale is to consider two populations of segments within each chain: the first population consists of the segments at each end of the polymer chain, which have fully relaxed on the time scale τ_r and are isotropically oriented; the second population consists of the central segments of each polymer chain, which relax on the time scale τ_d and are thus oriented for much longer times. The average orientation of the system $<P_2>_{system}$ is the average of these two populations, where $f/2$ is the fraction of segments at each end of the chain that have fully relaxed:

$$\langle P_2\rangle_{system} = f\langle P_2\rangle_{population\ 1} + (1-f)\langle P_2\rangle_{population\ 2} \quad (2)$$

In order to simulate these partially relaxed chains, population 1 is allowed to sample local configurations independent of orientation and has an average orientation $<P_2>_{population\ 1} \approx 0$; population 2 is then constrained to have an average orientation of approximately $<P_2>_{system}/(1-f)$, where $<P_2>_{system}$ corresponds to the observed birefringence. Depending on the value of f, even a modest value of $<P_2>_{system}$ may indicate very high degrees of orientation for the inner segments of the chain. The orientation along the contour of the chain using this two-population model is shown schematically in Fig. 1.

While the addition of chain contour fluctuation represents an improvement in the ability of the DE model to explain the loss of orientation in polymer chains, this model of relaxation is still an oversimplification and somewhat inexact [17]. Nevertheless, the addition of a contour fluctuation to the DE tube model reproduces qualitatively the observed phenomenon of a rapid loss of orientation at the chain ends, followed by the slower loss of orientation throughout the remainder of the chain [13]. We proceed on the basis of well-separated relaxation times, for which two distinct conditions suffice to describe approximately the structure for $\dot{\gamma}\tau_d > 1$: the first is the case of the uniformly oriented chain ($f=0$) for $\dot{\gamma}\tau_r > 1$; the second case is that of a chain relaxed to the extent described by Eq. (1) for $\dot{\gamma}\tau_r < 1$.

2.2. Application to polystyrene

It has been demonstrated [8,18] that the characterization of oriented samples of polystyrene by birefringence is insufficient to account for variations in the Young's modulus E_{11}. This has been explained by the fact that birefringence measures the average local orientation of the polymer chain, and is insensitive to any kind of inhomogeneity in orientational order, such as that arising from the relaxation of chain ends. The experiments of De Francesco and Duckett [8,9] considered systems of MW = 130–210 kg/mol and $T - T_g = 3$–28 K. Each sample was stretched uniaxially to 2, 4 or 6 times its initial gauge length in an Instron tensile instrument at constant cross-head speed of 10 mm/min, at a temperature slightly higher than T_g, and then quenched immediately for subsequent mechanical tests. Thus, samples deformed to larger total strain remain at high temperature longer and experience lower true strain rates than those deformed to smaller total strain. The time constants for these systems covered a broad range: $\tau_e = 0.05$–425 sec, $\tau_r = 9.0\times10^0$–1.0×10^5 sec, and $\tau_d = 3.0\times10^2$–9.0×10^6 sec. For any given molecular weight and temperature, an order of magnitude or more separates these time constants; this separation is more pronounced for the higher MW systems since $\tau_e \sim MW^0$, $\tau_r \sim MW^2$, and $\tau_d \sim MW^3$. For a given molecular weight, the time constants all increase by a factor of about 15 as $T - T_g$ decreases from 28 to 18 K. There is a more rapid increase as temperature nears T_g; the time constants increase by a factor of 10 over the smaller decrease of $T - T_g$ from 8 to 3 K (c.f. Table 3 of Ref. [9]). This illustrates the tremendous influence of temperature on the relaxation of polymers, especially as T approaches T_g.

To study the partial chain relaxation hypothesis proposed, we model four of the drawn PS samples produced by De Francesco and Duckett, all of which exhibited a birefringence $\Delta n \approx -0.014$ [8,9]. The details of these samples are shown in Table 1. We model these samples using $f=0$ for the samples with larger $\dot{\gamma}\tau_r/\lambda$ and $f \neq 0$ for the samples with smaller $\dot{\gamma}\tau_r/\lambda$, where $\dot{\gamma}$ is the initial strain rate and λ is the nominal draw ratio of the sample; in the latter case, $f=0.5$ for the 130 kg/mol sample and 0.4 for the 180 kg/mol sample, according to Eq. (1).

2.3. Molecular representation of PS

For a polymeric system comprised of N atoms or sites, distributed among N_{ch} chains, the Cartesian coordinate of the ith site of the jth chain can be written $\mathbf{r}_{i,j}$. Considering only the backbone of the chain, the intramolecular coordinates are

Table 1
Characteristics of samples produced by De Francesco and Duckett and modeled in this work

MW_n (kg/mol)	Nominal draw ratio, λ	T (K)	τ_r (s)	$\dot{\gamma}\tau_r/\lambda$	$-\Delta n$	E (GPa)
130	3	378	6.9×10^4	275	0.0125	2.65
130	5.5	383	6.4×10^3	14	0.0125	3.25
180	3	378	1.2×10^5	470	0.0155	2.70
180	4.5	383	1.1×10^4	28	0.0157	3.27

From Refs. [8,9]. $\dot{\gamma}$ is the initial strain rate of 0.012 s^{-1} applicable for all samples.

equivalently represented in terms of connector vectors $\mathbf{q}_{i,j}^{(m)}$ of the n_j sites along the backbone in each chain, where the superscript m indicates the number of bonds spanned by the connector. As in our previous work, we employ a "local chain direction" $\mathbf{q}_{i,j}^{(2)}$ defined as follows:

$$\mathbf{q}_{i,j}^{(2)} = \mathbf{r}_{i+1,j} - \mathbf{r}_{i-1,j}, \quad i = 2, 3, \ldots, n_j - 1 \tag{3}$$

Additionally, for polystyrene we define a unit vector $\mathbf{q}_{i,j}^{(\mathrm{p})}$ normal to the plane of the phenyl ring in the side group. Both of these vectors are shown in Fig. 2.

The description of the polystyrene (PS) chains in terms of $\mathbf{q}_{i,j}^{(2)}$ and $\mathbf{q}_{i,j}^{(\mathrm{p})}$ is motivated by the relationship between available experimental measurements and the physical organization of the molecules. Not only birefringence measurements, but also measurements of IR and Raman produce results that depend on the orientation of these vectors through the value of the second Legendre polynomial $P_2^{(m)}$ of the direction vectors shown in Fig. 2:

$$P_2^{(m)} = \frac{3\left(q_{ij,x}^{(m)}\right)^2}{2\left(q_{ij}^{(m)}\right)^2} - \frac{1}{2} \tag{4}$$

The birefringence $\triangle n$ is defined as [19]:

$$\Delta n = \frac{2\pi}{9}\frac{N}{V}\frac{(n^2+2)^2}{n}\left(\alpha_{xx} - \frac{\alpha_{yy}+\alpha_{zz}}{2}\right)\langle P_2\rangle = \Delta n_{\max}\langle P_2\rangle \tag{5}$$

where n is the refractive index of the material, N/V is the number density of birefringent units, and $\{\alpha_{xx}, \alpha_{yy}, \alpha_{zz}\}$ are the diagonal components of the polarizability tensor of the birefringent unit in its own principle frame of reference.

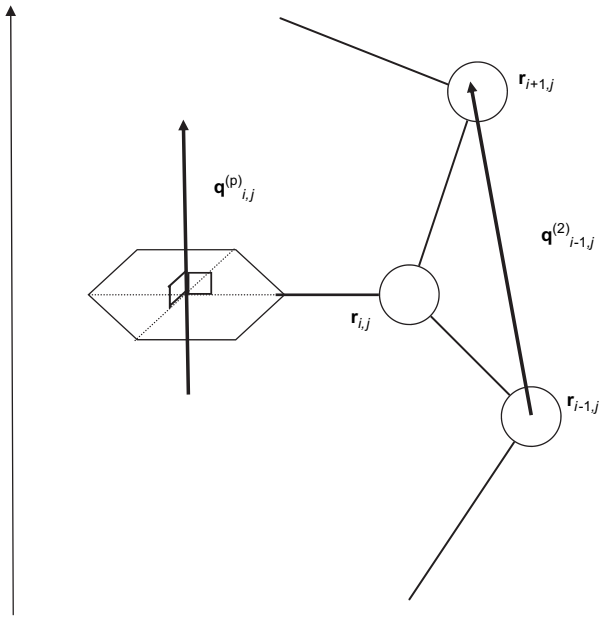

Fig. 2. Vectors used to define the orientation of a polystyrene chain.

In general, the orientation of the phenyl rings are expected to mirror that of the chain backbone, since $\mathbf{q}^{(2)}$ and $\mathbf{q}^{(\mathrm{p})}$ are parallel in the energetically favored conformation of the styrene unit. However, libration of the phenyl rings leads to a reduction in orientational order for the rings relative to that of the chain backbone, so the overall birefringence must be written as the sum of the contributions of the phenyl ring and the backbone. For polystyrene, the individual birefringences $\Delta n_{\max}$ for the chain backbone and the phenyl rings were calculated according to Eq. (5) using the traceless polarizability tensors of Abe et al. [20], which represent the anisotropy of polarizability for the backbone ($\alpha_{xx} = 1.741$, $\alpha_{yy} = -0.953$, $\alpha_{zz} = -0.788$) and the phenyl ring ($\alpha_{xx} = -2.981$, $\alpha_{yy} = 0.383$, $\alpha_{zz} = 2.598$), using a refractive index for PS of $n = 1.59$ for both [21]. This leads to the relationship between Δn and the orientational order parameters for the chain backbone $<P_2^{(2)}>$ and phenyl ring $<P_2^{(\mathrm{p})}>$:

$$\Delta n = \frac{N}{V}\left[23.5\left\langle P_2^{(2)}\right\rangle - 40.2\left\langle P_2^{(p)}\right\rangle\right] \tag{6}$$

where N/V is the number density of monomer units in Å^{-3}.

3. Simulation procedure

The force field used in these simulations is based on the united-atom model proposed by Mondello et al. [22]. They showed that this united-atom force field successfully reproduces two independent sets of X-ray data for PS within experimental error. In the united-atom force field, each carbon and associated hydrogens of the PS molecule are lumped together into a single site and labeled as indicated in Fig. 3. In order to adapt the Mondello force field to our existing code, the bond lengths along the backbone of the polymer were modeled as harmonic springs rather than as rigid bonds. The force constant was chosen to be consistent with the General Amber Force Field of Wang et al. [23], and did not introduce any

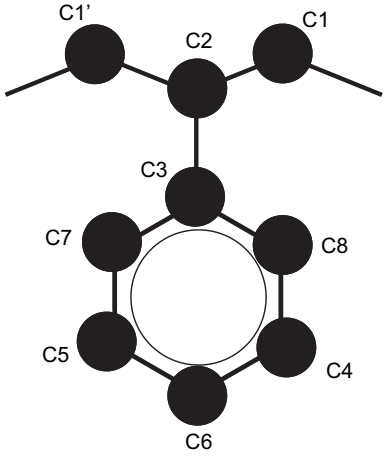

Fig. 3. Diagram of nomenclature for a styrene monomer.

significant changes in the average bond lengths and angles. The force field is as follows:

$$U = \sum_{\substack{\text{backbone}\\ \text{bonds}}} \frac{1}{2}k_b(b_i - b_0)^2 + \sum_{\substack{\text{backbone}\\ \text{angles}}} \frac{k_\theta}{2\sin^2\theta}(\cos\theta_i - \cos\theta_0)^2 + \sum_{\substack{\text{backbone}\\ \text{torsions}}} \frac{1}{2}k_\phi[1-\cos 3\phi_i] + \sum_{\text{rings}}\left\{\sum_{i=1,3} k_{\xi,i}\left(\xi_i - \xi_{0,i}\right)^2 + k_{oop}\varphi_i^2 + k_\chi(\chi_i - \chi_0)^2 + k_\tau\cos^2(\tau_i - \tau_0)\right\} + \sum_{\text{sites } i,j} 4\varepsilon\left[\left(\frac{\sigma}{r_{ij}}\right)^{12} - \left(\frac{\sigma}{r_{ij}}\right)^{6}\right] \quad (7)$$

In the equation above, the first term is the harmonic bond stretching potential, applied to the backbone bonds, where $b_0 = 0.153$ nm and $k_b = 3761$ kJ/mol/nm^2. The C–C bonds in the phenyl ring were fixed at 0.140 nm and the C2–C3 bond connecting the phenyl ring to the chain backbone was fixed at 0.151 nm. The second term is the harmonic bond angle bending potential, applied only to the C–C–C angles in the chain backbone. For the angle C1′–C2–C1, $\theta_0 = 1.91$ rad and $k_\theta = 502.1$ kJ/mol; for the angle C2′–C1–C2, $\theta_0 = 1.91$ rad and $k_\theta = 527.2$ kJ/mol. The C–C–C angles in the phenyl ring were fixed at 2.095 rad. The third term is the backbone torsion potential, which accounts for all intramolecular interactions between atoms separated by three bonds; ϕ_i is defined to be zero in the *trans* state and $k_\phi = 5.86$ kJ/mol. The fourth through seventh terms are specific to the phenyl rings. The fourth term arises due to bending of the phenyl ring relative to the chain backbone and has three contributions per ring: $\xi_{0,i} = 1.91$ rad and $k_{\xi,i} = 502.1$ kJ/mol/rad^2 for bond angle C1–C2–C3; $\xi_{0,i} = 2.095$ rad and $k_{\xi,i} = 585.8$ kJ/mol/rad^2 for bond angles C2–C3–C7 and C2–C3–C8. The fifth term is the out-of-plane bending energy, where φ_i is the angle defined by C2–C3–C6 and $k_{oop} = 334.7$ kJ/mol/rad^2. The sixth term is the improper torsion, which serves to maintain the chirality of the molecule. χ_i is the angle between the normal to the plane defined by C1′–C2–C1 and the bond C2–C3. Depending on the chirality of the C2 site, the equilibrium angle χ_0 will be either 0.6116 rad or 2.530 rad. The force constant is $k_\chi = 209.2$ kJ/mol/rad^2. The seventh term is the ring torsion, where τ_i is defined by projection onto the plane normal to C2–C3 of the angle between the normal to the ring, and the vector connecting sites C1 and C1′, and $k_\tau = 8.37$ kJ/mol with $\tau_0 = 1.571$ rad. The last term is the Lennard–Jones (LJ) potential, which is used to compute the nonbonded interactions between all united-atom pairs that are on different chains or that are separated by four or more bonds on the same chain. The nonbonded potential parameters are: C1, $\sigma = 0.385$ nm and $\varepsilon = 0.5021$ kJ/mol; C2, $\sigma = 0.370$ nm and $\varepsilon = 0.3766$ kJ/mol; CX, X ≠ 1,2, $\sigma = 0.370$ nm and $\varepsilon = 0.5021$ kJ/mol. Lorentz–Berthelot mixing rules were used for interactions between all unlike sites. The cut-off distance for all nonbonded interactions was 0.770 nm, or twice the largest value of σ. A corresponding long-range correction based on $g(r) = 1$, where $g(r)$ is the radial distribution function between any pair of atom types, was applied to the simulation.

The polymer chains were 30-mers long, regio-regular head-to-tail, atactic with a *meso* dyad fraction of 0.5 ± 0.03, and terminated with a CH_3 group at each end. Thus, each molecule had 61 backbone sites and 30 phenyl rings, for a total of 241 sites/molecule. Each individual system consisted of four such chains. Because of the difficulty of sampling phase space in the glassy state, all results were averaged over six independent simulations. The root mean squared values of the radius of gyration $\langle r_g^2\rangle^{1/2}$ for samples of 40-mer and 80-mer polystyrenes were also simulated to confirm agreement in conformational properties between our simulations and those of Lyulin and Michels [24], who also used a version of the Mondello force field, modified to relax the rigidity of the phenyl ring angles.

The acceptance criterion for the SGMC simulation of uniaxially oriented molecules employed in this work differs from the corresponding isotropic *NPT* simulations by the addition to the Hamiltonian of the measure of chain backbone anisotropy, $P_2^{(2)}$, and its thermodynamic conjugate, the scalar physical potential μ. The relative probability of a configuration is related to the thermodynamic variables as follows:

$$\ln(p) \propto -\beta\left[U(r^N) + PV - \mu\sum_{i,j} P_2^{(2)}\right] + N\ln V \quad (8)$$

The value of $P_2^{(p)}$ was not constrained since the time scale of ring libration (i.e., the β relaxation) is much faster than that of the chain backbone. Addition of a term containing $P_2^{(p)}$ to Eq. (8) was found to bias the orientation of the rings relative to the chain backbone, thus producing improbable conformations.

For the purposes of mechanical property determination, the $[N\sigma T\mu]$ ensemble was used, with the following Hamiltonian:

$$\ln(p) \propto -\beta\left[U(r^N) + \sum \sigma_{z'}A_{x'y'}(\ell_{z'} - \ell_{z',0}) - \mu\sum_{i,j} P_2^{(2)}\right] + N\ln V \quad (9)$$

where $[x',y',z']$ was cycled over $[x,y,z]$, $[y,z,x]$, and $[z,x,y]$; the axes of the simulation box were kept orthogonal. The change in the normal stress difference attributable to the applied physical potential (μ) was determined according to the Eq. (A3) of Ref. [3]. Because the strains were small, $\langle P_2^{(2)}\rangle$ did not change significantly, and the contribution of this term to the stress was unimportant.

Simulations of homogeneously oriented systems (using Eq. (8)) were run for $\langle P_2^{(2)}\rangle_{system} = 0.0$, 0.1, 0.2, 0.3, 0.4 and 0.5. Simulations of inhomogeneously oriented systems that account for the partial loss of orientation at the chain ends were run for $\langle P_2^{(2)}\rangle_{system} = 0.3$ and $f = 0.0$, 0.4 and 0.5. All

simulations were run in four stages: (1) generation of independent configurations that match the target $<P_2^{(2)}>_{system}$ through the application of an appropriate value of μ for PS "ghost" chains (i.e., with LJ potentials turned off), called "amorphization"; (2) application of the LJ potentials to equilibrate the PS melt at the target $<P_2^{(2)}>_{system}$ at $T = 550$ K in the $[NPT\mu]$ ensemble, called "melt equilibration"; (3) generation of glassy samples using a series of $[NPT\mu]$ simulations by reducing temperature from 550 to 300 K while the value of the physical potential μ was continuously updated to maintain $<P_2^{(2)}>_{system}$ constant, called "quench"; and (4) evaluation of the elastic modulus using the relationship between stress and strain obtained from simulations with five applied stresses σ_x, ranging from −30 to 30 MPa in the $[N\sigma T\mu]$ ensemble, called "glass deformation".

In each of stages (1)–(3), the physical potentials (μ) were iterated using a procedure reported by Bathe and Rutledge [25], based on the method developed by Lyubartsev and Laaksonen [26]; for inhomogeneously oriented systems ($f \neq 0$) the potential μ was applied only to population 2, the central fraction $(1-f)$ of the chain. Stage 1 was run for 20,000 MC cycles; stage 2 was run for 175,000–250,000 cycles; the temperature was reduced in stage 3 from 550 to 300 K over 750 steps of 200 cycles each; elastic properties were evaluated in stage 4 over 450,000 cycles. Because the systems rapidly lose orientation in the absence of the applied physical potential, the value of μ obtained from the cooling stage was applied and held constant during the application of stress in stage 4. The equilibration was judged on the basis of a stable value of orientation without drift in the value of μ for stages 1 and 2; in subsequent stages, convergence of volume and energy was used as an indicator of equilibration. Table 2 summarizes the simulation protocol described above.

During any given simulation, the following Monte Carlo moves were employed: (1) site translation, (2) reptation, (3) re-bridging, (4) end rotation, (5) pendant move, and (6) volume change. Other than the pendant move, all of these moves were performed as described previously [3]. The added pendant move attempts at random to perturb one of the following: a ring torsion, an out-of-plane bending angle, an improper torsion, or a ring bending angle. The maximum sizes of these perturbations were continuously updated to maintain 50% acceptance. The attempt frequency and typical fraction of accepted moves (for the isotropic melt) were, respectively: site translation, 0.44 and 0.50; reptation, 0.11 and <0.001; re-bridging, 0.11 and 0.01; end rotation, 0.11 and 0.50; pendant move, 0.22 and 0.50.

Table 2
Simulation protocol

Stage	Simulation parameters
1: Amorphization	$T = 550$ K
	$\mu \Rightarrow$ iterated (see text)
2: Melt equilibration $[NPTN_{ch}\mu]$	$P = 0.1$ MPa
	$T = 550$ K
	$\mu \Rightarrow$ iterated (see text)
3: Quench $[NPTN_{ch}\mu]$	$P = 0.1$ MPa
	300 K $< T <$ 550 K
	$\mu \Rightarrow$ iterated (see text)
4: Glass deformation $[N\sigma TN_{ch}\mu]$	$\sigma_y = \sigma_z = 0.1$ MPa
	$\sigma_x - \sigma_y$ (MPa) $= -30, -15, 0\ 15, 30$
	$T = 300$ K
	$\mu \Rightarrow$ value from previous step

The decorrelation times of the end-to-end vectors for polystyrene are extremely long compared to our earlier polyethylene simulations, due in large part to the absence of variable connectivity moves, which were found to be ineffective for PS due to the presence of the large phenyl side group. A similar problem was previously encountered with variable connectivity moves for polypropylene, and resolved through the use of an expanded ensemble in Hamiltonian space [27]; this was not attempted here. The longest relaxation time, and consequently the time for orientation to react to the application of a given μ (i.e., for orientation to propagate throughout the polymer chain), scales as the square of the chain length, n_j^2. Thus, a trade-off was necessary between the length of chain that could be equilibrated practically in an oriented state, and the length of chain required to obtain quantitative estimates of mechanical properties (as evident below). The current simulations of 30-mer PS were each run in parallel over the course of several weeks on 1.6 MHz Pentium processors; these 30-mers were sufficient to reproduce realistic densities and orientation in the glassy state.

As an aside, the original Mondello force field was developed using simulations in the *NVT* ensemble and was not confirmed to yield the correct pressure. In applying this force field to studies of 80-mers of polystyrene in the *NPT* ensemble, Lyulin and coworkers found it necessary to introduce a pressure correction in order to match the melt phase density. Even so, the density of the polymer glass so obtained underestimates the experimental density by about 2% (see Fig. 3 of Ref. [24]); as reported below, our simulation densities range from about 3% above to 2% below the same set of experimental values. Since we obtain comparable agreement with the experimental density data in the glassy state for these 30-mers, we used the force field without this pressure correction.

4. Results and discussion

4.1. Melt configurations

The ensemble average chain orientations are shown in Fig. 4 as a function of the applied potential for the melt equilibration stage. The absolute values of μ obtained at the end of the cooling stage did not differ significantly from those of the melt stage; however, due to lack of ergodic sampling at the lower temperatures of the glassy state, these μ values should be viewed only as "locally relevant" to a particular region of phase space at low temperature. Since μ was iterated to maintain a specific orientation for each sample, there is a distribution of values corresponding to each value of $<P_2>$. For the PS melt, Fig. 4 is analogous to Fig. 1 of Ref. [3]. For the value of $<P_2>_{system} = 0.3$, we observe that the μ values applied to the central $(1-f)$ portion of the chain tend to be

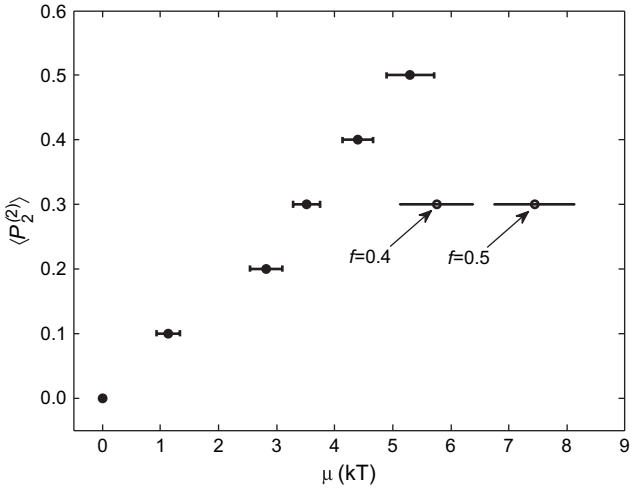

Fig. 4. Ensemble orientation of chain orientation $<P_2^{(2)}>_{system}$ as a function of orientation potential μ obtained during melt equilibration. Filled circles represent the $f = 0.0$ systems; the open circles represent the $f \neq 0.0$ systems as labeled. Bars represent the range of values for μ that produced the specified values of $<P_2>_{system}$.

slightly larger than the μ value for the homogeneous system simply corrected by $(1 - f)$.

Fig. 5 shows the distribution of orientation as a function of position along the chain, for the cases of a homogeneously oriented system ($f = 0$) and an inhomogeneously oriented system ($f = 0.5$), generated during the melt equilibration stage. The most important aspect of Fig. 5 is that the average distributions indicate effective sampling of the possible conformations at each level of orientation and at each position along the chain. As can be seen, the application of the physical potential is very effective in creating the desired orientation distribution; the resulting plots may be compared with the hypothesized cases shown in Fig. 1. However, the use of a single position-independent orientation potential μ throughout the chain does create some artifacts in the contour orientation. This is most apparent for the orientation at the chain ends and for the abrupt transition between the oriented and isotropic portions for the case of $f = 0.5$. The value of μ may, in general, depend on the proximity of the segment to the chain ends or intramolecular correlations of the chain in the vicinity of a change in local orientation. Due to the connectivity of the chains, these effects are distributed over several segments and account for the curvature in the orientation distributions. These effects could be corrected using a chain position-dependent μ, but this was not done here.

4.2. Glass transition

Fig. 6 shows a cooling curve for the isotropic polystyrene melt obtained from the quench stage. From this, we estimate a T_g of 415 ± 30 K for this model of polystyrene using data between 300 and 500 K. This is somewhat higher than the value of 380 K obtained by Lyulin et al. [28]. This difference is most likely due to the addition of the pressure correction term and the lower density obtained by Lyulin and Michels [24], as discussed above. Although our results indicate a high value for the glass transition, it is also noteworthy that the T_g is sensitive to the range of data used for the determination of the melt phase coefficient of thermal expansion, because of the large volume change and the rapid quench

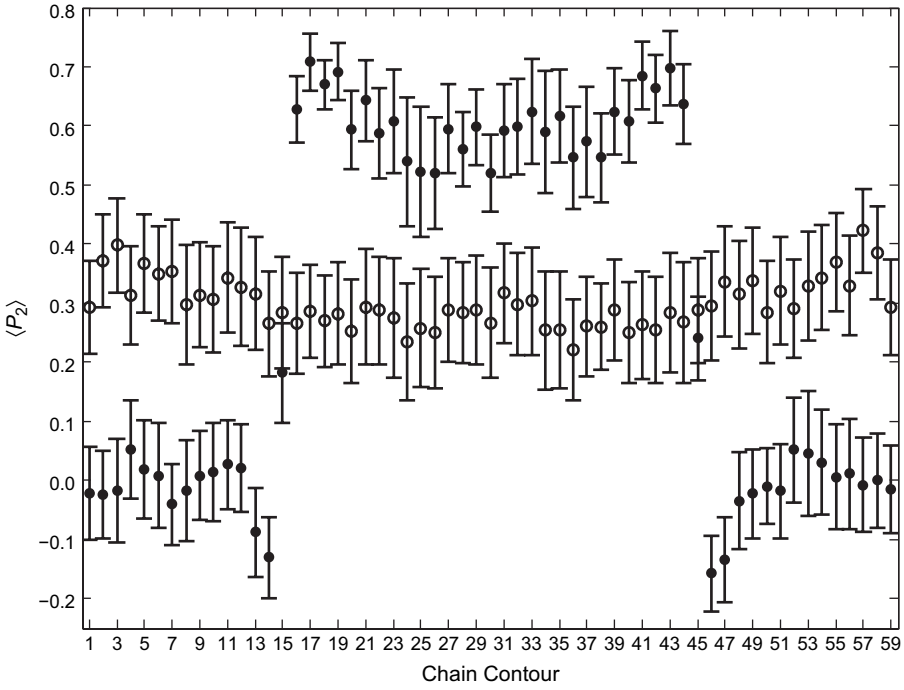

Fig. 5. Ensemble average orientation over the chain contour for $<P_2>_{system} = 0.3$: $f = 0.0$ (open circles) and 0.5 (filled circles) during the melt equilibration stage. The chain contour represents the 59 $\mathbf{q}^{(2)}$ vectors along the chain.

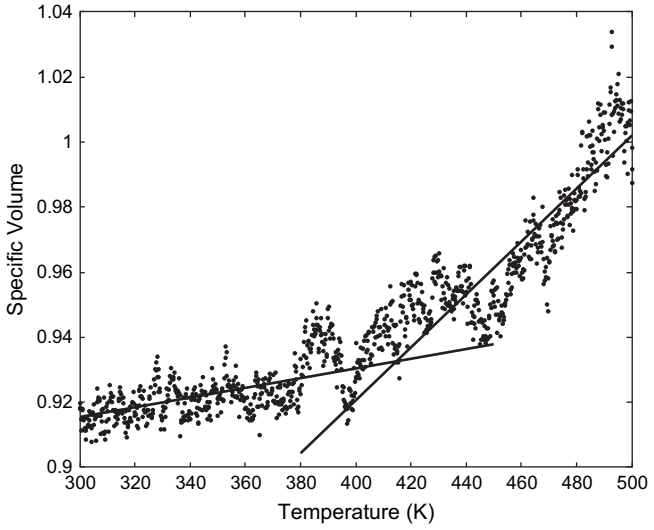

Fig. 6. Cooling curve for atactic PS, MW = 3135 g/mol (30-mers). The resulting T_g is approximately 415 ± 30 K. Lines were fitted using data from 300 to 360 K for the glassy regime and from 420 to 500 K for the melt regime.

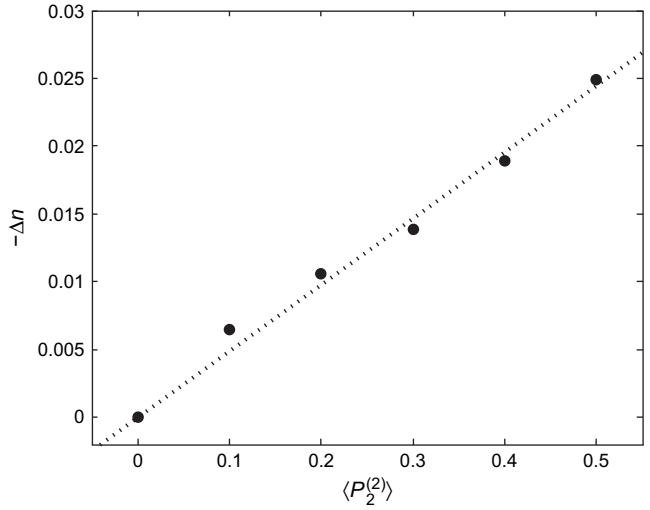

Fig. 7. Birefringence as a function of the chain orientation. Dashed line represents a linear least squares regression of the birefringences obtained for each value of chain orientation.

rate; excluding values above 480 K provides a glass transition temperature of about 390 K, which is very close to the expected value of 380 K.

The density obtained for glassy polystyrene chains of 30-mers and 80-mers at 300 K was about 1.08 g/cm^3, comparable to the literature value of 1.05 g/cm^3 for PS [29]; simulations of polystyrene chains of 20-mers gave a density of 0.95 g/cm^3, which was deemed to be too low to be representative of polystyrene. The densities obtained through our simulations ranged from 1.08 to 1.03 g/cm^3, with the oriented systems generally having lower density compared to the isotropic system.

4.3. Birefringence

Fig. 7 shows the variation of birefringence with orientation for the homogeneously oriented systems. The overall birefringence was obtained using Eq. (5) with the coefficients obtained from Abe [20] and the orientation averages independently obtained from the simulations. By extrapolation to $<P_2> = 1.0$, we obtain a value of Δn_{max} (the value of birefringence at full orientation) equal to −0.0489. This is in excellent agreement with the value of −0.048 obtained by Vancso et al. using WAXS and birefringence [30] from a similar study of the relationship between birefringence and average chain orientation over this same range.

4.4. Elasticity of homogeneously oriented polystyrene

The determination of the modulus E_{11} was made from the results of the [$N\sigma T\mu$] simulations through fitting to the relationship:

$$\sigma_1 = E_{11}\varepsilon_1 \tag{10}$$

where $\varepsilon_1 = \delta L_x/L_{x0}$ and atmospheric pressure was maintained in the lateral directions, y and z. Voigt notation is used for Young's modulus. The strains obtained from the simulations spanned the range +/−1.0% for the most oriented PS systems, and +/−2.0% for the isotropic systems, well within the range of elastic behavior for PS [31].

Fig. 8 shows the increase of the Young's modulus E_{11} with increasing birefringence, or equivalently $<P_2>$, for simulations with homogeneously distributed orientation, $f = 0$. Looking first at the results for simulations without any orientational bias, i.e., $-\Delta n = 0$, the simulated value is $E_{11} = 1.7$ GPa. This falls significantly below experimental values of the isotropic Young's modulus, which are typically in the range of 2.3–3.3 GPa [29]. However, additional simulations of 80-mer PS predict a modulus of 2.3 GPa for the isotropic case, which agrees significantly better with the experimental values and with the value of 2.9 GPa obtained by MD simulations of 160-mer chains at the same temperature by Lyulin et al. [32]. From this, we conclude that the downward shift of 0.8 GPa for the simulation results using 30-mer PS are due to the low molecular weight, relative to the experimental systems.

Secondly, Fig. 8 also shows the variation of the simulated modulus with increasing birefringence. Despite the downward shift relative to the experimental data attributed to molecular weight mismatch, the trend in modulus with increasing birefringence agrees well with the trend in the experimental data of De Francesco and Duckett [8], in particular the trend associated with lower bound of modulus versus birefringence, since these result from the systems with lowest strain ratio λ, and thus correspond closest to the $f = 0$ case. The simulated values of the modulus increase by 1.2 GPa between $-\Delta n = 0$ and 0.025, compared to approximately 1.6 GPa for the experimental data over the same range. As mentioned earlier, the decision to simulate 30-mers was made as the result of a trade-off between practical considerations required for accurate equilibration of orientation and quantitative accuracy of properties such as density for the isotropic system. The

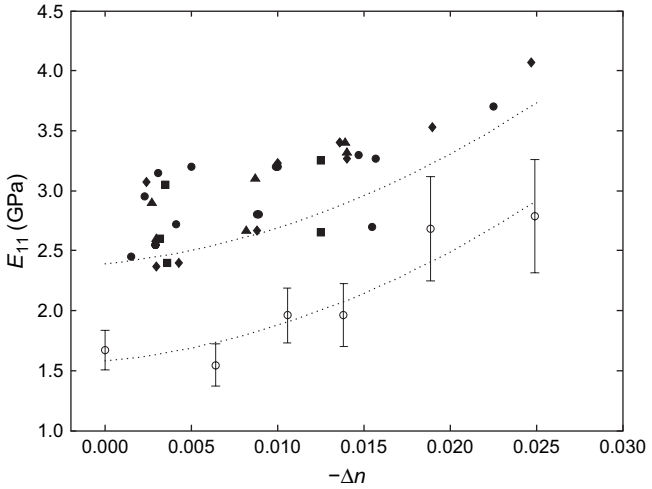

Fig. 8. Increase of tensile modulus with the birefringence from simulations and experiments. Simulations assuming homogeneously oriented ($f = 0$) 30-mer PS (open circles); experimentally observed measures of tensile modulus versus birefringence for samples of PS with MW = 130 kg/mol (filled squares), 150 kg/mol (filled diamonds), 180 kg/mol (filled circles), and 210 kg/mol (filled triangles), reproduced from Figs. 3 and 4 of Ref. [8]. Variation in the moduli can be attributed to the processing conditions, as explained in the text. The dashed lines represent guides to the eye. The lower dashed line is drawn to show the increase of modulus with birefringence from simulations; the upper dashed line represents the best fit of the lower line to the lower bound of experimental data. The shift is 0.8 GPa.

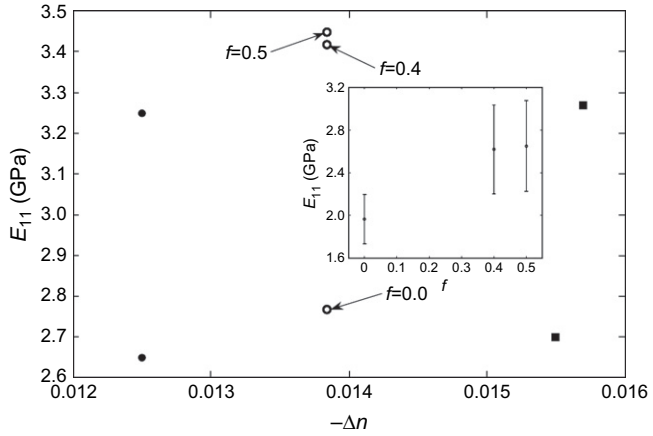

Fig. 9. Modulus as a fraction of chain inhomogeneity for simulations having $<P_2>_{system}$ approximately equal to 0.3 ($\Delta n = -0.0139$). The choices of experimental data points, and the determination of values of f, are described in the Section 2.2. The plot shows shifted data for simulations (open circles), and experimental data for MW = 130 kg/mol, $f = 0$ or 0.5 (filled circles) and for MW = 180 kg/mol, $f = 0$ or 0.4 (filled squares); for the experimental data, the higher modulus corresponds to the larger strain ratio λ in both cases. The inset shows the uncorrected values of modulus for the simulations as a function of f, including standard deviation.

downward shift in mechanical properties appears to be systematic and entirely due to molecular weight. Nevertheless, we believe these results are promising with regard to the ability of the SGMC method to reproduce the relationship between two macroscopically observable quantities, birefringence and tensile Young's modulus.

4.5. Elasticity of inhomogeneously oriented polystyrene

In order to explain the range of modulus values they observed for samples with similar birefringence, De Francesco and Duckett [8] hypothesized the presence of inhomogeneities in the distribution of the backbone orientation of the chain, as originally proposed by Doi [10]. The tensile moduli obtained by De Francesco and Duckett [8] are shown in Fig. 8. At any given birefringence, samples that were more highly drawn at a higher temperature exhibited a higher modulus. De Francesco and Duckett [8] concluded that the existence of inhomogeneity in the chain is responsible for the increase in the mechanical properties, i.e., that the increase in modulus due to a more highly oriented center of the chain more than offsets the decrease due to less highly oriented chain ends. Fig. 9 shows the increase in modulus with the increase of the fraction of chain f with relaxed orientation for the cases singled out in Section 2.2. For purposes of comparison, the simulation results are shifted by 0.8 GPa to compensate for the average downward shift of the 30-mer moduli. The increase of the modulus due to inhomogeneous orientation predicted by the simulations is consistent with the increase in the modulus observed experimentally for samples drawn to large strain ratio at high temperature [8]. These results suggest that it is the fractional orientation of the chain, rather than the actual length of chain or number of entanglements, that is responsible for the observed increases in modulus.

For comparison, we provide an analysis of the relationship between the distribution of orientation and mechanical properties using the Aggregate Model of Ward [33]. This model describes a polymer system as an aggregate of identical, non-interacting mechanical units. Parameterization proceeds by equating the mechanical properties of an individual unit to that of the fully oriented material. The mechanical properties of the aggregate can thus be expressed as a function of the orientation distribution of the individual mechanical units. The Aggregate Model predicts that the change in the modulus with increasing f at a fixed birefringence is proportional to the quantity $(2s_{13} + s_{66} - s_{11} - s_{33})$, where the s_{ij} are compliance constants in Voigt notation. Experimental estimates of this quantity for PS indicate that it is negative [2,34,35]. This means that the Aggregate Model predicts a decrease of E_{11} with increasing $<P_2^{(2)}>_{\text{population 2}}$ at constant $<P_2^{(2)}>_{\text{system}}$, in contradiction to the experimental results and the simulations reported here. This qualitative difference underscores the value of atomistic simulations to understand phenomena such as the effect of the distribution of orientation on the mechanical properties of polymers.

5. Conclusion

There are three novel aspects to the methodology presented here to analyze the connection between the structural and mechanical properties of PS. First, there is the use of an atomistic-level Monte Carlo method (as opposed to the previous molecular dynamics (MD) reports) to probe the properties of

glassy PS. Second, there is the ability to constrain the orientation of the polymer chains to mimic the observed birefringence of the PS glass. Third, there is application of orientation constraints either homogeneously or inhomogeneously throughout the simulation cell. This method is remarkable in that it allows us to study systems characterized by partially relaxed orientation on the time scale of τ_r, which can easily be on the order of minutes to hours, well beyond anything remotely possible using MD. This provides the opportunity for a more complete understanding of the effects of microstructure on the mechanical properties.

The simulation results obtained here for oriented PS support long-standing observations that mechanical properties improve with orientation, as characterized by birefringence. While the simulated moduli are low by 0.8 GPa due to limitations on the MW simulated, the trend in modulus with birefringence is quantitatively accurate. The simulation results furthermore provide evidence for the explanation of De Francesco and Duckett [8] that the variation of modulus with processing conditions for samples of comparable birefringence is due to partial relaxation in the more highly-drawn, high temperature systems. Significantly, the simulations reproduce the experimentally observed increase of the tensile modulus by assuming inhomogeneity of orientation due to partial relaxation of the PS chains.

Atomistic simulations are shown to be particularly useful in the case of PS, because they provide qualitatively different results from the behavior predicted by the Aggregate Model. We believe this difference is indicative of the importance of the distribution of orientation along the chain and the nature of interactions between different parts of the chain. The importance of the atomic-level interactions is not unique to PS, and we expect that the additional information provided through atomistic simulation will similarly provide insight into the structural problems of other polymers. Because of its flexibility, the SGMC methodology can be tailored to produce spatial, or other, heterogeneities, thereby providing the tools to investigate a wide variety of polymer structural problems at the atomic level. This ability to mimic conditions inaccessible by direct MD simulation provides not only the means to evaluate their structural thermodynamic properties, but also a starting point for MD simulations to probe their dynamic properties.

References

[1] Hadley DW, Pinnock PR, Ward IM. J Mater Sci 1969;4:152.
[2] Wright H, Faraday CSN, White EFT, Treloar LRG. J Phys D Appl Phys 1971;4:2002.
[3] Bernardin FE, Rutledge GC. Macromolecules 2007;40:4691.
[4] Bernardin FE, Rutledge GC. Macromol Theor Sim, submitted for publication.
[5] Rutledge GC. Phys Rev E 2001;63:021111.
[6] Dreher S, Seifert S, Zachmann HG, Moszner N, Mercoli P, Zanghellini G. J Appl Polym Sci 1998;67:531.
[7] Somani RH, Yang L, Hsiao BS. Polymer 2006;47:5657.
[8] De Francesco A, Duckett RA. Polymer 2004;45:8005.
[9] De Francesco A, Duckett RA. Polymer 2004;45:4297.
[10] Doi M. J Polym Sci Polym Phys Ed 1983;21:667.
[11] Milner ST, McLeish TCB, Likhtman AE. J Rheol 2001;45:2.
[12] Doi M. J Chem Soc Faraday Trans 2 1979;75:32.
[13] Tassin JF, Monnerie L, Fetters LJ. Macromolecules 1988;21:2404.
[14] Doi M, Edwards SF. Theory of polymer dynamics. New York: Oxford University Press; 1986 (section 7.4.2).
[15] des Cloizeaux J. J Phys Lett 1984;45:17.
[16] Needs RJ. Macromolecules 1984;17:437.
[17] Watanabe H. Prog Polym Sci 1999;24:1253.
[18] Carey DA, Wust CJ, Bogue DC. J Appl Polym Sci 1980;25:575.
[19] Riande E, Saiz E. Dipole moments and birefringence of polymers. Englewood Cliffs, NJ: Prentice-Hall; 1992.
[20] Abe Y, Tonelli AE, Flory PJ. Macromolecules 1970;3:294.
[21] Bicerano J. Prediction of polymer properties. New York: Marcel Dekker; 2002.
[22] Mondello M, Yang H-J, Furuyu H, Roe R-J. Macromolecules 1994;27:3566.
[23] Wang J, Wolf R, Caldwell J, Kollman P, Case D. J Comput Chem 2004;25:1157.
[24] Lyulin AV, Michels MAJ. Macromolecules 2002;35:1463.
[25] Bathe M, Rutledge GC. J Comput Chem 2003;24:876.
[26] Lyubartsev AP, Laaksonen A. Phys Rev E 1995;52:3730.
[27] Kuppa VK, in 't Veld PJ, Rutledge GC. Macromolecules 2007;40:5187.
[28] Lyulin AV, Vorselaars B, Mazo MA, Balabaev NK, Michels MAJ. Europhys Lett 2005;618:71.
[29] Modern plastics encyclopedia '99, vol. 75(12). Modern Plastics; 1998. p. B207.
[30] Vancso G, Snétivy D, Tomka I. J Appl Polym Sci 1991;42:1351.
[31] Chow TS. Polymer 1993;34:541.
[32] Lyulin AV, Li J, Mulder T, Vorselaars B, Michels MAJ. Macromol Symp 2006;237:108.
[33] Ward IM. Proc Phys Soc 1962;80:1176.
[34] Hughes DS, Kelly JL. Phys Rev 1953;92:1145.
[35] Kruger JK, Grammes C, Stockem K, Zietz R, Dattenmaier M. Colloid Polym Sci 1991;269:764.